

A compact inorganic layer for robust anode protection in lithium-sulfur batteries

Yu-Xing Yao¹ | Xue-Qiang Zhang¹ | Bo-Quan Li¹ | Chong Yan² | Peng-Yu Chen¹ | Jia-Qi Huang²  | Qiang Zhang¹ 

¹Beijing Key Laboratory of Green Chemical Reaction Engineering and Technology, Department of Chemical Engineering, Tsinghua University, Beijing, China

²Advanced Research Institute of Multidisciplinary Science, Beijing Institute of Technology, Beijing, China

Correspondence

Qiang Zhang, Beijing Key Laboratory of Green Chemical Reaction Engineering and Technology, Department of Chemical Engineering, Tsinghua University, Beijing 100084, China.

Email: zhang-qiang@mails.tsinghua.edu.cn

Funding information

Tsinghua University Initiative Scientific Research Program; National Natural Science Foundation of China, Grant/Award Numbers: U1801257, 21825501, 21676160; National Key Research and Development Program, Grant/Award Numbers: 2015CB932500, 2016YFA0202500

Abstract

Lithium-sulfur (Li-S) batteries are one of the most promising candidates for high energy density rechargeable batteries beyond current Li-ion batteries. However, severe corrosion of Li metal anode and low Coulombic efficiency (CE) induced by the unremitting shuttle of Li polysulfides immensely hinder the practical applications of Li-S batteries. Herein, a compact inorganic layer (CIL) formed by *ex situ* reactions between Li anode and ionic liquid emerged as an effective strategy to block Li polysulfides and suppress shuttle effect. A CE of 96.7% was achieved in Li-S batteries with CIL protected Li anode in contrast to 82.4% for bare Li anode while no lithium nitrate was employed. Furthermore, the corrosion of Li during cycling was effectively inhibited. While applied to working batteries, 80.6% of the initial capacity after 100 cycles was retained in Li-S batteries with CIL-protected ultrathin (33 μm) Li anode compared with 58.5% for bare Li anode, further demonstrating the potential of this strategy for practical applications. This study presents a feasible interfacial regulation strategy to protect Li anode with the presence of Li polysulfides and opens avenues for Li anode protection in Li-S batteries under practical conditions.

KEYWORDS

electrochemical energy storage, lithium metal anode, lithium-sulfur batteries, rechargeable battery, solid electrolyte interphase

1 | INTRODUCTION

Batteries with high energy densities have been a long-term pursuit in multiple fields, such as electric vehicles, unmanned drones, and portable electronics.¹⁻⁴ Despite the great success of lithium-ion batteries (LIBs) in the past 30 years, the energy density of LIBs is approaching the theoretical limit, providing a huge impetus for the research of emerging battery chemistries.⁵⁻⁷ Lithium-sulfur (Li-S) batteries have attracted worldwide

attention in recent years^{8,9} because the combination of the most energy-dense Li metal as anode and earth-abundant, high-specific capacity S as cathode creates an overwhelming theoretical energy density of 2600 Wh kg⁻¹. Li-S batteries are regarded as a suitable candidate to replace LIBs for next-generation energy storage systems.¹⁰

However, the development of Li-S batteries is strongly hindered by a series of issues including the insulating nature of cathode active materials, the notorious “shuttle effect” of Li polysulfides,¹¹ and subsequent Li corrosion.¹² Currently, the corrosion of Li anode gradually becomes the actual

Yu-Xing Yao and Xue-Qiang Zhang contributed equally to this study.

This is an open access article under the terms of the Creative Commons Attribution License, which permits use, distribution and reproduction in any medium, provided the original work is properly cited.

© 2019 The Authors. *InfoMat* published by John Wiley & Sons Australia, Ltd on behalf of UESTC.

bottleneck that limits the overall performance of Li-S batteries as the advancement of S cathode design, especially under practical conditions.¹³⁻¹⁵ The corrosion of Li metal can be attributed to the following two reasons: (a) Li metal is highly reactive toward almost all nonaqueous solvents and Li salts in nature, generating solid electrolyte interphase (SEI) on the surface of Li anode.¹⁶ Moreover, dendritic Li forms and cracks the fragile SEI during Li plating.^{17,18} The rupture of SEI aggravates the side reactions between Li and electrolyte. The nonstopping side reactions deteriorate the utilization efficiency of Li anode and cycling performance of batteries.¹⁹ (b) Soluble Li polysulfides shuttle between S cathode and Li anode, causing severe corrosion of Li anode and loss of active materials in Li-S batteries.²⁰ The continuous corrosion of Li anode and rapid depletion of electrolyte are the main culprits for the failure of Li-S batteries, especially with high sulfur loadings ($>4 \text{ mg cm}^{-2}$) and slightly excess Li.²¹ Therefore, protecting Li anode from the side reactions induced by electrolytes and Li polysulfides is critical for promoting the further development of Li-S batteries under practical conditions.²²⁻²⁴

A key prerequisite for a Li anode protection layer in Li-S batteries is that Li must be protected in the presence of Li polysulfides compared with the battery systems adopting insoluble intercalation cathodes.²⁵⁻²⁷ Li polysulfides react with Li and involve into SEI constituents, which complexes the interfacial chemistry on Li anodes and invalidates most of the common SEI design strategies, posing great challenges for effective Li protection. Therefore, constructing SEI that concurrently blocks Li polysulfides and suppresses side reactions with Li is imperative. Generally, SEI on Li anode composes of both inorganic and organic species, as it is the result of the decomposition of both Li salts and organic solvents.¹⁶ SEI can be divided into two layers according to dominant components at different depths.²⁸⁻³⁰ The organic layer is porous and soluble, making it susceptible to polysulfide attacking. The inorganic layer is compact but conductive, which can be tailored to block Li polysulfides and protect Li anode.

An effective strategy for Li anode protection layer in Li-S batteries is to employ SEI-forming additives, such as LiNO_3 ,³¹⁻³⁵ lithium polysulfides,³⁶⁻³⁸ SOCl_2 ,³⁹ and sulfur-containing polymers.^{40,41} Additives react irreversibly with Li anode to form in situ protective layer, in which the role of inorganic components is realized.⁴²⁻⁴⁵ However, the sacrificial nature of the film-forming additives cripples their effects during long-term cycling. Constructing a robust ex situ protective layer emerges as another effective way to protect Li anode.⁴⁶ For instance, Chen et al prepared a lithium phosphorus oxynitride (LiPON) layer on Li metal anode using plasma-enhanced electron beam evaporation for anode protection in Li-S batteries⁴⁷ and demonstrated that such LiPON layer can block the reactions between Li anode and polysulfides. Zhang

et al⁴⁸ proposed an implantable SEI for Li anode protection by an electrochemical method prior to cycling, which is compatible with S and high-voltage cathodes with enhanced performance. Nevertheless, the cost and process complexity in previous works have to be taken into considerations for practical Li-S batteries. Therefore, a facile but effective method to construct a protection layer on Li anode is strongly requested to block Li polysulfides and improve the performance of Li-S batteries under practical conditions.

In this article, a compact inorganic layer (CIL) was constructed ex situ on Li anode by the spontaneous reactions between Li and ionic liquid (IL) precursor composed of 0.5 M lithium bis(fluorosulfonyl)imide (LiFSI) dissolved in 1-butyl-3-methylimidazolium nitrate ([BMIM][NO₃]) IL (Figures 1A and S1). IL owns great potential in electrochemical applications due to several unique properties such as negligible vapor pressure, wide electrochemical window, and exceptional thermal stability.^{49,50} In contrast to routine nonaqueous electrolytes, the IL precursor consists solely of cations and anions and is solvent free. The absence of organic solvents and the chemical stability of [BMIM] cation

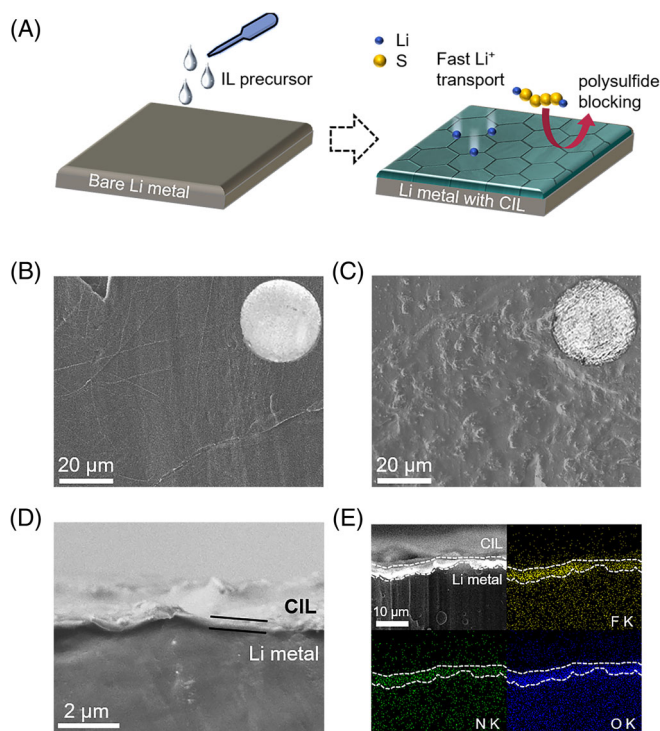


FIGURE 1 Schematic illustrations of the formation of CIL on Li anode and SEM images of Li and CIL. A, CIL is constructed by simply dripping IL precursor on Li anode. The spontaneous reactions between Li and IL render an CIL to block Li polysulfides. Top SEM views of, A, bare and, C, CIL-Li anodes. The insets are optical images of the corresponding Li plates. D, Cross-sectional view and, E, the corresponding EDS mapping of CIL. CIL, compact inorganic layer; CIL-Li, CIL-protected Li; EDS, energy-dispersive X-ray spectroscopy; IL, ionic liquid; SEM, scanning electron microscopy

renders SEI with anion-derived components. The employment of 0.5 M LiFSI in [BMIM][NO₃] as IL precursor allows the exposure of Li metal to FSI⁻ anions and super-concentrated (5.76 M by calculation) NO₃⁻ anions. NO₃⁻ is known as an excellent SEI precursor widely applied in Li metal batteries^{51,52} and the decomposition of FSI⁻ is proven to form LiF-rich SEI with high surface energy,^{53,54} rendering a CIL on Li anode. The as-formed CIL is able to block polysulfides, thus enabling a highly stable Li metal anode even under harsh test conditions. A Coulombic efficiency (CE) of 96.7% was achieved in Li-S batteries with CIL-protected Li (CIL-Li) anode in contrast to 82.4% for bare Li anode while no lithium nitrate was employed. Furthermore, 80.6% of initial capacity is retained in Li-S batteries with CIL-protected ultrathin (33 μm) Li anode compared with 58.5% for bare Li anode after 100 cycles.

2 | RESULTS AND DISCUSSION

The surface morphology of bare Li anode (denoted as bare Li) and CIL-Li metal was characterized using scanning electron microscopy (SEM). Bare Li exhibits a smooth surface, corresponding to the silver color of Li metal plate (Figure 1B). After dipping Li metal in IL precursor for 24 hours to form CIL, the color of Li metal plate turns dark and the generation of a surface film is clearly observed (Figure 1C), which indicates the formation of a conformal layer on Li metal. Cross-sectional SEM view reveals that CIL has a thickness of roughly 400 nm (Figure 1D) and is tightly adhered to the Li metal anode. The composition of CIL was obtained by the in-built energy-dispersive X-ray spectroscopy in SEM (Figure 1E). The fluorine (F) mapping indicates that CIL contains a considerable amount of F, and F element is only found in CIL. Nitrogen and oxygen are concentrated at the top CIL even though there are nitrogen and oxygen in both bulk Li metal because Li metal inevitably reacts with air during sample transfer process. Therefore, CIL mainly consists of inorganic fluorides, nitrides, and oxides, but more detailed chemical information needs to be probed.

X-ray photoelectron microscopy (XPS) with Ar⁺ sputtering was employed to investigate the chemical compositions of CIL along its depth (Figure 2). Compared with bare Li, an increasing N, O, and F content and low C content indicate the inorganic nature of CIL-Li (Figure S2). There is only one peak with a binding energy of 534.0 eV at 0 minute for O 1s spectra (Figure 2A), representing the N—O or O—S bond in the NO₃⁻ and FSI⁻ anions. As the surface etching continues, a 530.9 eV peak for Li₂O emerges as the reduction product of anions at 0.5 minute and further increases till 2.0 minutes. F 1s spectra follow the same trend (Figure 2B), exhibiting a F—S peak (688.6 eV) at the surface and strengthening LiF (684.6 eV) peak in the inner part as a result of F—S reduction

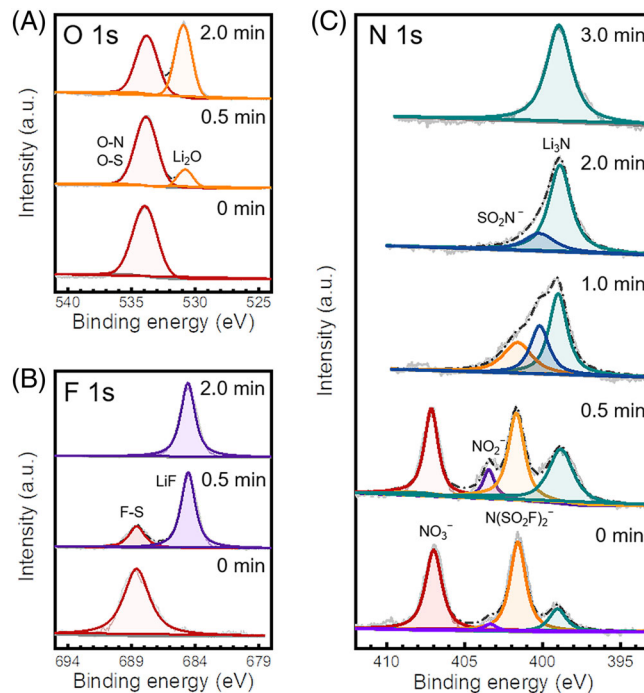
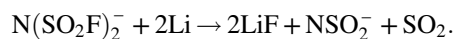
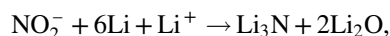
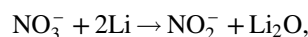


FIGURE 2 Surface chemistry of CIL probed by XPS. A, O 1s, B, F 1s, and C, N 1s spectra at different etching times. CIL, compact inorganic layer; XPS, X-ray photoelectron microscopy

by Li metal. The high mechanical modulus and surface energy of LiF were proven to suppress Li dendrites in previous publications.⁵⁵⁻⁵⁷ N 1s spectra exhibits four peaks at the surface due to its strong oxidizing nature (Figure 2C), namely, NO₃⁻ (407.0 eV), N(SO₂F)₂⁻ (401.6 eV), and their reduction products NO₂⁻ (403.3 eV) and Li₃N (399.0 eV). NOS₂⁻ (400.1 eV) emerges after 1.0 minute of etching.^{58,59} As etching continues, all N species converts to Li₃N which has an ultrahigh ionic conductivity of 10⁻³ to 10⁻⁴ S cm⁻¹, thus enabling fast Li-ion transport through CIL.⁶⁰ Based on these results, CIL is mainly composed of Li₂O, LiF, and Li₃N as inorganics and the possible reaction mechanisms of the decomposition of IL precursor in contact with Li metal are also proposed:



In order to test the long-term cycling stability of CIL-Li, Li-Li symmetrical cells are assembled using different electrolytes (Figure 3A). In carbonate-based electrolytes, Li metal anode tends to form massive dendrites and is notoriously unstable (Figure S3a,b). The voltage hysteresis of

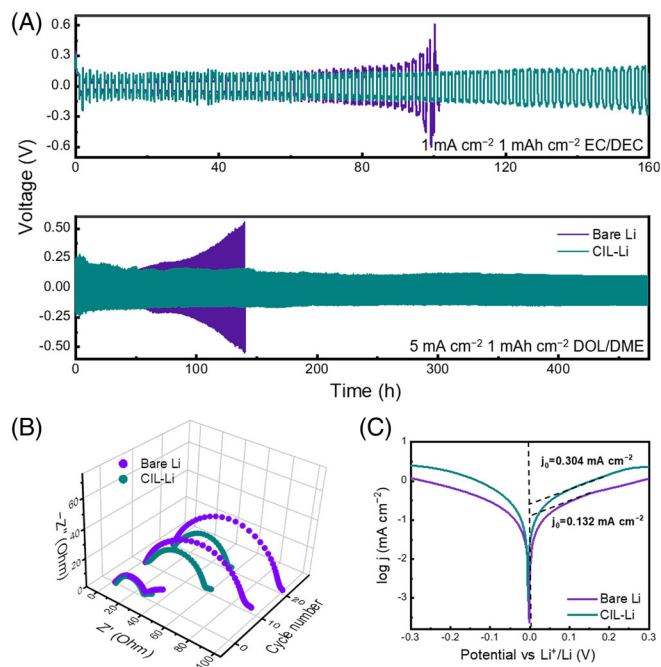


FIGURE 3 Long-term cycling stability and ion-transport properties of CIL-Li anode. A, Voltage profiles of Li-Li symmetrical cells cycled in different electrolytes. B, EIS measurements taken after various cycle numbers in EC/DEC electrolyte. C, Tafel curves and derived exchange current density obtained from linear sweep voltammetry tests in the range of -0.3 V to 0.3 V at 1 mV s^{-1} . CIL-Li, compact inorganic layer-protected Li; EC/DEC, ethylene carbonate/diethyl carbonate; EIS, electrochemical impedance spectroscopy

bare Li is relatively stable in the first 80 hours, then sharply increases to 0.6 V followed by short circuit at a current density of 1 mA cm^{-2} and a capacity of 1 mAh cm^{-2} . This can be attributed to the dendrite penetration through the separator. However, a stable operation of 160 hours with only slightly increased polarization is observed and dendrites are clearly suppressed with a protective CIL (Figures S3c,d and S4a). The CIL-Li exhibits a more remarkable performance in ether-based electrolyte under a large current density of 5 mA cm^{-2} , maintaining a stable polarization of $\sim 120 \text{ mV}$ for more than 470 hours (Figure S4b). In contrast, bare Li exhibits an ever-increasing polarization until the cell open circuits due to the accumulation of dead Li. The excellent long-term stability of CIL-Li anode is the premise for stable operation of Li-S batteries.

The surface chemistry of CIL-Li after cycling was particularly investigated to gain insights into the reason of its excellent stability. For Li anodes cycled in carbonate electrolyte (Figure S5), XPS spectra of C 1s from the surface down to 10.0 minutes etching depth are presented in Figure S6a,b. There are various C-containing species derived from the decomposition of solvents on bare Li surface. This can be attributed to the break, rebuild, and accumulation of SEI as

carbonate solvents continuously decompose. By sharp contrast, C 1s signal becomes undetectable after 3.0 minutes of etching for CIL-Li, indicating that solvent decomposition is strongly restrained and CIL effectively protects fresh Li from electrolyte corrosion. For Li anodes cycled in ether electrolyte, the XPS spectra of F 1s of bare Li show Li-F and C-F bond while no obvious N 1s signal can be detected (Figure S7a,b). The formation of C-F bond can be attributed to the solvent decomposition, indicating that the routine SEI cannot effectively prevent solvent penetration and subsequent side reactions. By sharp contrast, XPS spectra of CIL-Li after cycling exhibit solely LiF and Li₃N signals without any organic species, indicating that CIL successfully suppresses the solvent corrosion of Li anode and the composition of CIL maintains unchanged (Figure S7c,d). The inhibition of the side reactions between Li and electrolytes suggests that CIL is compact, chemically, and electrochemically stable in nature, which is essential for blocking Li polysulfides in working Li-S batteries.

A protective layer for Li anode must ensure adequate Li ion diffusion through itself while blocking shuttle species. To further understand the ion transport features of the CIL, a symmetrical cell composed of bare Li as the reference and counter electrode, CIL-Li as the working electrode was assembled and a series of electrochemical tests were conducted. Electrochemical impedance spectroscopy (EIS) before and after cycling were measured (Figure 3B) and the corresponding Nyquist plots were fitted using the equivalent circuit shown in Figure S8. The initial SEI resistance (R_{SEI}) of CIL-Li is comparable to bare Li, but the R_{SEI} resistance for bare Li sharply increases from 25.8 to 89.6Ω after cycling, while CIL-Li only slightly increases from 23.7 to 38.5Ω . Tafel plots obtained from the cyclic voltammetry (CV) test (Figures 3C and S9) confirm that the exchange current density of CIL-Li (0.304 mA cm^{-2}) is more than two times as bare Li (0.132 mA cm^{-2}), which is in accordance with the greater current response observed in the CV test. The reduction of interfacial resistance and high exchange current density signify that CIL possesses a higher Li-ion conductivity compared to routine SEI.

Li anode with CIL protection was further evaluated in working Li-S batteries. The tests were designed to be carried out under two harsh conditions: ultrathin Li foil as anodes and LiNO₃-free electrolytes. In conventional Li-S batteries test, thick Li metal plates (typically $>500 \mu\text{m}$) with sufficient Li reservoir are applied and batteries can achieve long cycles even if Li is continuously consumed. The cycling data of such batteries mainly depend on cathode properties and the true electrochemical performance of Li anode is concealed. Therefore, ultrathin Li metal anode ($33 \mu\text{m}$, 6.6 mAh cm^{-2}) was used in all Li-S tests in this work, aiming to evaluate the

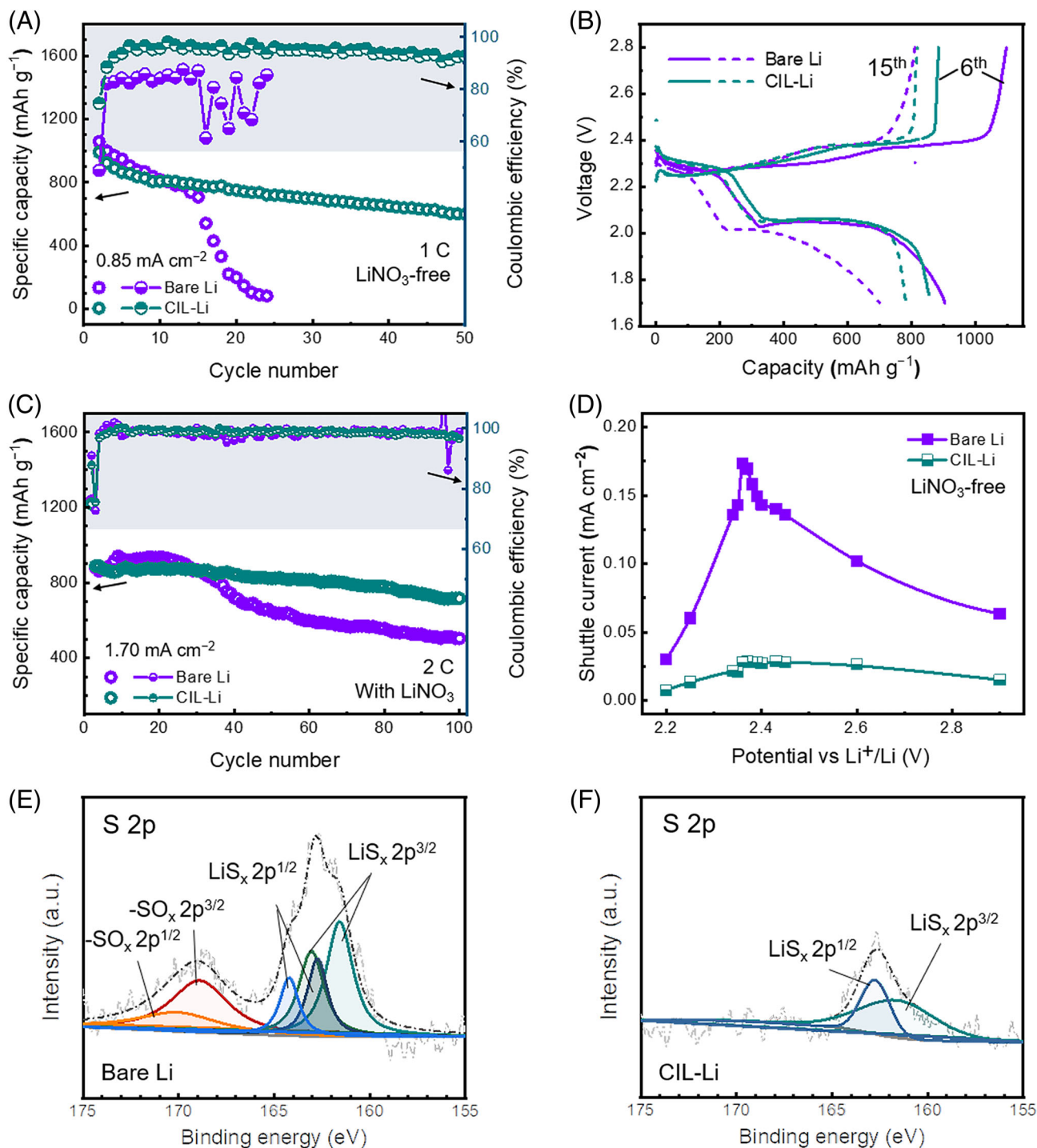


FIGURE 4 Electrochemical performance of Li-S batteries with ultrathin Li anode and Li surface chemistry after cycling. A, Galvanostatic cycling of Li-S batteries in LiNO₃-free electrolyte at 1 C and, B, corresponding voltage profiles at the 6th and 15th cycles. C, Galvanostatic cycling of Li-S batteries in LiNO₃-containing electrolyte at 2 C. D, Shuttle current measurements at different voltages ranging from 2.2 to 2.9 V using LiNO₃-free electrolyte. S 2p XPS spectra of, E, bare Li and, F, CIL-Li after 5 cycles in Li-S batteries containing LiNO₃-free electrolyte. CIL-Li, compact inorganic layer-protected Li; XPS, X-ray photoelectron microscopy

effect of anode protection and disclose the real performance of Li anode under practical conditions. LiNO₃ has been widely applied in Li-S batteries as an indispensable additive for shuttle effect inhibition and dendrite suppression.^{31-33,51,61}

Once removing LiNO₃ in ether-based electrolytes, Li-S batteries display much deteriorated performance. Therefore, the effect of CIL can be examined without any interference in a LiNO₃-free Li-S battery. By employing LiNO₃-free

electrolytes (Figure 4A), bare Li is incapable of stopping polysulfide shuttle, exhibiting an initial CE of merely 82.2% and typical overcharge (Figure 4B). The cell fails after 15 cycles along with the depletion of Li anode, which originates from the severe side reactions between Li and polysulfides. CIL-Li demonstrates a high initial CE of 96.7% and an average CE of 94.8% in the following 50 cycles, showing much smaller polarization

and minor capacity decay. It can be calculated that an average 0.44 mAh cm^{-2} of Li is consumed during each cycle for bare Li, taking up as much as ca. 55% of the total cell capacity. For CIL-Li, only an average $0.132 \text{ mAh cm}^{-2}$ Li is consumed irreversibly through each cycle, suggesting that CIL protects Li anode from the corrosion of polysulfides and significantly enhance the anode reversibility. Moreover, CIL-Li anode exhibits

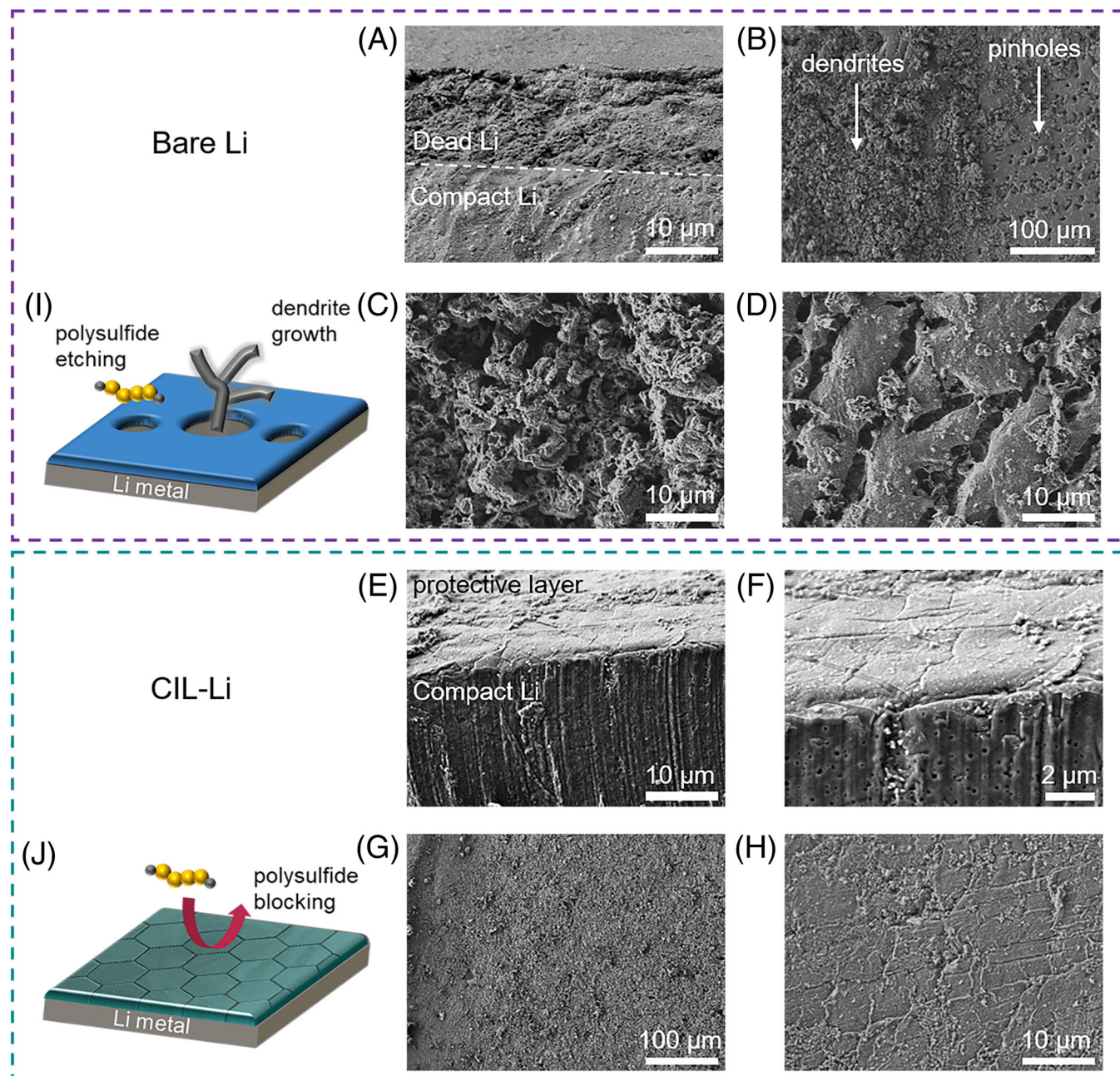


FIGURE 5 SEM images of Li metal anode after 5 cycles in LiNO_3 -free Li-S batteries. A, Cross-sectional and, B, top view of bare Li anode at charging state at the fifth cycle, showing two distinct features: C, dendrite growth and, D, surface corrosion by Li polysulfides. E, Cross-sectional and, G, top view of CIL-Li anode. F,H, The magnified images in E and G, showing a dendrite-free, intact protective layer. I,J, Schematics of the corresponding surface properties of bare Li and CIL-Li anode. CIL-Li, compact inorganic layer-protected Li; SEM, SEM, scanning electron microscopy

superior cycling performance compared to unprotected Li anodes with the presence of LiNO_3 . The introduction of LiNO_3 effectively improves the cycle performance of bare Li at a demanding rate of 2 C, but rapid cell fade still occurs after 30 cycles and the capacity retention by the end of 100 cycles is merely 58.5% with an average CE of 98.6% (Figures 4C and S10). This can be attributed to the breakage of LiNO_3 -induced SEI under large current densities and subsequent polysulfide corrosion. As comparison, CIL-Li retains 80.6% of its initial capacity after 100 cycles and exhibits a high average CE of 98.8%. The superior performances of Li-S batteries under harsh conditions including ultrathin anode, LiNO_3 -free electrolytes, and high-rate cycling firmly verify the high efficacy of CIL in robust Li metal anode protection against Li polysulfides.

The excellent electrochemical performance of Li-S batteries with CIL-Li anode can be attributed to Li polysulfides blocking, which was carefully investigated using quantitative electrochemical method and surface chemistry analysis. The shuttle currents at different potentials were directly probed using constant potential amperometry. A distinct current peak occurs at 2.36 V for bare Li, signifying the strongest polysulfide shuttle induced by the most soluble Li_2S_6 species at this potential. As comparison, CIL-Li shows no current peak at all potentials, and its shuttle current density at 2.36 V is reduced by six times compared to bare Li anode. The appreciable decrease of shuttle current indicates the suppression of polysulfide shuttle and subsequent inhibition of the side reactions between Li anode and polysulfides, which was clearly proved by the surface chemistry analysis of Li anodes after cycling. XPS of Li anode was carried out after five cycles in LiNO_3 -free Li-S batteries (Figures 4E, F and S11). According to Li 1s and S 2p spectra, bare Li is covered by a series of S-containing species including $-\text{SO}_x$ and LiS_x while CIL-Li only exhibits much weaker LiS_x peaks. The reduction of $-\text{SO}_x$ species for CIL-Li can be attributed to both the prevention of lithium bis(trifluoromethanesulfonyl)imide (LiTFSI) decomposition and scarcity of LiS_x species because it may evolve $-\text{SO}_x$ species through oxidation, and the reduction of LiS_x species indicates that less LiS_x is generated from the reactions between Li and polysulfides. It can be concluded that CIL effectively blocks the majority of diffusing polysulfides and restrains the side reactions, thus leading to much improved Li-S battery performance.

The blocking of Li polysulfides and the inhibition of Li corrosion induced by CIL were further visualized by SEM. After five cycles in LiNO_3 -free electrolyte, dead Li starts to accumulate (Figure 5A) and the surface clearly demonstrates two distinct patterns on bare Li metal anode caused by polysulfide attacking (Figure 5B-D): the mossy dendritic morphology and large numbers of pinholes and cracks. On the

opposite, dead Li is reduced significantly and a compact, intact protective layer maintains on the top surface for CIL-Li (Figure 5E-H). The surface evolution of bare Li and CIL-Li can be depicted by schematics (Figure 5I,J). During cycling, the surface erosion of bare Li is caused by Li polysulfides, which destroys the original flat surface, undermines the uniformity of SEI, and creates lots of pinholes. Therefore, the formation and growth of Li dendrites prevail, causing rapid accumulation of dead Li and battery fade. CIL-Li anode blocks the majority of the polysulfides and suppresses the corrosion of Li, maintaining the original surface and SEI for uniform Li deposition and finally ensuring Li-S batteries with exceedingly long lifespan.

3 | CONCLUSIONS

In conclusion, a CIL constructed by employing a feasible pretreatment method was proposed to protect Li anode in Li-S batteries, in particular with ultrathin Li anode. The CIL is capable of blocking Li polysulfide shuttling and suppressing the corrosion of Li due to the abundant inorganic components and compact structure. Therefore, Li-S batteries with CIL-Li anode achieve a CE up to 96.7% compared to 82.4% for bare Li with no LiNO_3 additives. Moreover, the corrosion of Li during cycling is effectively relieved, and 80.6% of the initial capacity after 100 cycles retains for Li-S batteries with CIL-protected ultrathin (33 μm) Li anodes in contrast to 58.5% for bare Li anode. This study demonstrates an inspiring route to protect Li anode with the presence of Li polysulfides, which opens avenues for high energy, ultra-stable Li-S batteries under practical conditions.

4 | EXPERIMENTAL SECTION

4.1 | Materials

Li metal plate (500 μm) and ultrathin Li metal foil (33 μm) were purchased from China Energy Lithium Co., Ltd. The carbonate-based electrolyte was prepared by adding 1 M LiPF_6 in a 1:1 (vol:vol) ethylene carbonate (EC)/diethyl carbonate (DEC) mixture. The ether-based electrolyte was prepared by adding 1 M LiTFSI in a mixture of 1:1 (vol:vol) 1,2-dimethoxyethane (DME) and 1,3-dioxolane (DOL). LiNO_3 of 2 wt% was added as an additive for Li-S battery testing. All solvents and LiFSI salt were purchased from TCI (Shanghai) Development Co., Ltd. [BMIM][NO_3] was purchased from Shanghai Aladdin Bio-Chem Technology Co., Ltd. For the preparation of IL precursor, 0.5 M LiFSI was directly dissolved in [BMIM][NO_3] to form a homogeneous solution. CIL was constructed by immersing Li metal in the IL precursor for 24 hours under room temperature and then

washed the residual IL with DME solvent. LiNO₃ and S were purchased from Alpha Aesar.

4.2 | Structure characterizations

The morphologies of the Li metal anodes were characterized by SEM (JSM 7401F, JEOL Ltd., Tokyo, Japan) operated at 3.0 kV, 10 μA. XPS spectra were obtained using PHI Quantera SXM (ULVAC-PHI, Inc., Kanagawa, Japan) with an AlK_α radiation (pass energy 55.0 eV) at a pressure lower than 10⁻⁷ Torr. All the Li anode samples were washed three times using pure DME to clean the surface residual Li salts and organic solvents. During transferring process before any characterization, all samples were protected in Ar-filled containers to avoid direct contact with air and moisture.

4.3 | Electrochemical measurements

The cathode of Li-S batteries in this article was prepared by blade-coating method. The S cathode was composed of S, conductive carbon nanotubes (CNTs), and poly(vinylidene fluoride) (PVDF) binder. Sulfur and CNTs were firstly mixed in a batch with a weight ratio of 7:3. The obtained composite was then mixed with the PVDF binder with a weight ratio of 9:1 in *N*-methyl-2-pyrrolidone under sonication and stirring to form a homogeneous suspension. The suspension was then coated on an Al current collector and dried at 60°C for 12 hours. All electrodes were dried under vacuum before use and punched into round pieces with a diameter of 13 mm. The mass loading of the S cathode is 1.0 mg cm⁻². Two-electrode cell configuration using standard 2032 coin-type cells was applied in all the electrochemical measurements and assembled in an Ar-filled glove box with O₂ and H₂O content below 0.1 ppm. The CV measurements were performed within the range of -0.3 to 0.3 V at a scanning rate of 1 mV s⁻¹. The EIS measurements were performed in frequencies ranging from 10⁵ to 1 Hz with a voltage amplitude of 5 mV. CV and EIS tests were conducted using Solartron 1470E electrochemical workstation (Solartron Analytical). The Li-S cells were cycled in galvanostatic mode within a voltage range 1.7-2.7 V, respectively. The Li-S batteries were all first activated at 0.2 C for one cycle prior to the following cycling at more demanding rates. Battery cycling tests were all conducted using LAND multichannel battery cyler (Wuhan LAND Electronics Co., Ltd.).

ACKNOWLEDGMENTS

This work was supported by National Key Research and Development Program (2016YFA0202500 and 2015CB932500), National Natural Science Foundation of China (21676160,

21825501, and U1801257), and the Tsinghua University Initiative Scientific Research Program.

ORCID

Jia-Qi Huang  <https://orcid.org/0000-0001-7394-9186>

Qiang Zhang  <https://orcid.org/0000-0002-3929-1541>

REFERENCES

1. Choi JW, Aurbach D. Promise and reality of post-lithium-ion batteries with high energy densities. *Nat Rev Mater.* 2016;1:16013.
2. Xin S, Chang ZW, Zhang XB, Guo Y-G. Progress of rechargeable lithium metal batteries based on conversion reactions. *Natl Sci Rev.* 2017;4:54.
3. Ju JW, Ma J, Wang YT, Cui Y, Han P, Cui G. Solid-state energy storage devices based on two-dimensional nano-materials. *Energy Storage Mater.* 2019;20:269-290.
4. Liang Y, Zhao CZ, Yuan H, et al. A review of rechargeable batteries for portable electronic devices. *InfoMat.* 2019;1:6-32.
5. Li M, Lu J, Chen Z, Amine K. 30 years of lithium-ion batteries. *Adv Mater.* 2018;30:1800561.
6. Winter M, Barnett B, Xu K. Before Li ion batteries. *Chem Rev.* 2018;118:11433-11456.
7. Lu Y, Rong X, Hu Y-S, Li H, Chen L. Research and development of advanced battery materials in China. *Energy Storage Mater.* <https://doi.org/10.1016/j.ensm.2019.05.019>.
8. Yin YX, Xin S, Guo YG, Wan LJ. Lithium-sulfur batteries: electrochemistry, materials, and prospects. *Angew Chem Int Ed.* 2013; 52:13186-13200.
9. Fang R, Zhao S, Sun Z, Wang DW, Cheng HM, Li F. More reliable lithium-sulfur batteries: status, solutions and prospects. *Adv Mater.* 2017;29:1606823.
10. Bruce PG, Freunberger SA, Hardwick LJ, Tarascon J-M. Li-O₂ and Li-S batteries with high energy storage. *Nat Mater.* 2011;11:19.
11. Li SY, Wang WP, Duan H, Guo YG. Recent progress on confinement of polysulfides through physical and chemical methods. *J Energy Chem.* 2018;27:1555-1565.
12. Zhang X-Q, Zhao C-Z, Huang J-Q, Zhang Q. Recent advances in energy chemical engineering of next-generation lithium batteries. *Engineering.* 2018;4:831-847.
13. Zhao Y, Ye Y, Wu F, Li Y, Li L, Chen R. Anode interface engineering and architecture design for high-performance lithium-sulfur batteries. *Adv Mater.* 2019;31:1806532.
14. Cao RG, Xu W, Lv DP, Xiao J, Zhang JG. Anodes for rechargeable lithium-sulfur batteries. *Adv Energy Mater.* 2015;5: 1402273.
15. Zhao Y, Goncharova LV, Sun Q, et al. Robust metallic lithium anode protection by the molecular-layer-deposition technique. *Small Methods.* 2018;2:1700417.
16. Peled E, Menkin S. Review—SEI: past, present and future. *J Electrochem Soc.* 2017;164:A1703-A1719.
17. Zhang R, Shen X, Cheng X-B, Zhang Q. The dendrite growth in 3D structured lithium metal anodes: electron or ion transfer limitation? *Energy Storage Mater.* <https://doi.org/10.1016/j.ensm.2019.03.029>.

18. Li Y, Huang W, Li Y, Pei A, Boyle DT, Cui Y. Correlating structure and function of battery interphases at atomic resolution using cryoelectron microscopy. *Joule*. 2018;2:2167-2177.
19. Cheng XB, Zhang R, Zhao CZ, Zhang Q. Toward safe lithium metal anode in rechargeable batteries: a review. *Chem Rev*. 2017;117:10403-10473.
20. Manthiram A, Fu Y, Chung SH, Zu C, Su YS. Rechargeable lithium-sulfur batteries. *Chem Rev*. 2014;114:11751-11787.
21. Peng HJ, Huang JQ, Cheng XB, Zhang Q. Review on high-loading and high-energy lithium-sulfur batteries. *Adv Energy Mater*. 2017;7:1700260.
22. Cheng XB, Yan C, Huang JQ, et al. The gap between long lifespan Li-S coin and pouch cells: the importance of lithium metal anode protection. *Energy Storage Mater*. 2017;6:18-25.
23. Zhang G, Peng HJ, Zhao CZ, et al. The radical pathway based on a lithium-metal-compatible high-dielectric electrolyte for lithium-sulfur batteries. *Angew Chem Int Ed*. 2018;57:16732-16736.
24. Wang Y, Sahadeo E, Rubloff G, Lin CF, Lee SB. High-capacity lithium sulfur battery and beyond: a review of metal anode protection layers and perspective of solid-state electrolytes. *J Mater Sci*. 2019;54:3671-3693.
25. Wang YZ, Huang XX, Zhang SQ, Hou Y. Sulfur hosts against the shuttle effect. *Small Methods*. 2018;2:1700345.
26. Zhang G, Zhang ZW, Peng HJ, Huang JQ, Zhang Q. A toolbox for lithium-sulfur battery research: methods and protocols. *Small Methods*. 2017;1:1700134.
27. Cheng XB, Huang JQ, Zhang Q. Review—Li metal anode in working lithium-sulfur batteries. *J Electrochem Soc*. 2018;165:A6058-A6072.
28. Yan C, Cheng XB, Tian Y, et al. Dual-layered film protected lithium metal anode to enable dendrite-free lithium deposition. *Adv Mater*. 2018;30:1707629.
29. Shi S, Lu P, Liu Z, et al. Direct calculation of Li-ion transport in the solid electrolyte interphase. *J Am Chem Soc*. 2012;134:15476-15487.
30. Gu Y, Wang W-W, Li Y-J, et al. Designable ultra-smooth ultra-thin solid-electrolyte interphases of three alkali metal anodes. *Nat Commun*. 2018;9:1339.
31. Aurbach D, Pollak E, Elazari R, Salitra G, Kelley CS, Affinito J. On the surface chemical aspects of very high energy density, rechargeable Li-sulfur batteries. *J Electrochem Soc*. 2009;156:A694.
32. Zhang SS. A new finding on the role of LiNO₃ in lithium-sulfur battery. *J Power Sources*. 2016;322:99-105.
33. Zhang SS. Role of LiNO₃ in rechargeable lithium/sulfur battery. *Electrochim Acta*. 2012;70:344-348.
34. Liang X, Wen Z, Liu Y, et al. Improved cycling performances of lithium sulfur batteries with LiNO₃-modified electrolyte. *J Power Sources*. 2011;196:9839-9843.
35. Xiong S, Xie K, Diao Y, Hong X. Properties of surface film on lithium anode with LiNO₃ as lithium salt in electrolyte solution for lithium-sulfur batteries. *Electrochim Acta*. 2012;83:78-86.
36. Zhao CZ, Cheng XB, Zhang R, et al. Li₂S₅-based ternary-salt electrolyte for robust lithium metal anode. *Energy Storage Mater*. 2016;3:77-84.
37. Li W, Yao H, Yan K, et al. The synergetic effect of lithium polysulfide and lithium nitrate to prevent lithium dendrite growth. *Nat Commun*. 2015;6:7436.
38. Zhang L, Ling M, Feng J, Mai L, Liu G, Guo J. The synergetic interaction between LiNO₃ and lithium polysulfides for suppressing shuttle effect of lithium-sulfur batteries. *Energy Storage Mater*. 2018;11:24-29.
39. Li S, Dai HL, Li YH, et al. Designing Li-protective layer via SOCl₂ additive for stabilizing lithium-sulfur battery. *Energy Storage Mater*. 2019;18:222-228.
40. Li G, Gao Y, He X, et al. Organosulfide-plasticized solid-electrolyte interphase layer enables stable lithium metal anodes for long-cycle lithium-sulfur batteries. *Nat Commun*. 2017;8:850.
41. Li G, Huang Q, He X, et al. Self-formed hybrid interphase layer on lithium metal for high-performance lithium-sulfur batteries. *ACS Nano*. 2018;12:1500-1507.
42. Zhang XQ, Chen X, Cheng XB, et al. Highly stable lithium metal batteries enabled by regulating the solvation of lithium ions in non-aqueous electrolytes. *Angew Chem Int Ed*. 2018;57:5301-5305.
43. Zhao Q, Tu ZY, Wei SY, et al. Building organic/inorganic hybrid interphases for fast interfacial transport in rechargeable metal batteries. *Angew Chem Int Ed*. 2018;57:992-996.
44. Li NW, Shi Y, Yin YX, et al. A flexible solid electrolyte interphase layer for long-life lithium metal anodes. *Angew Chem Int Ed*. 2018;57:1505-1509.
45. Shen X, Cheng X, Shi P, et al. Lithium-matrix composite anode protected by a solid electrolyte layer for stable lithium metal batteries. *J Energy Chem*. 2019;37:29-34.
46. Lin C-F, Qi Y, Gregorczyk K, Lee SB, Rubloff GW. Nanoscale protection layers to mitigate degradation in high-energy electrochemical energy storage systems. *Acc Chem Res*. 2018;51:97-106.
47. Wang WW, Yue XY, Meng JK, et al. Lithium phosphorus oxynitride as an efficient protective layer on lithium metal anodes for advanced lithium-sulfur batteries. *Energy Storage Mater*. 2019;18:414-422.
48. Cheng XB, Yan C, Chen X, et al. Implantable solid electrolyte interphase in lithium-metal batteries. *Chem*. 2017;2:258-270.
49. Armand M, Endres F, MacFarlane DR, et al. Ionic-liquid materials for the electrochemical challenges of the future. *Nat Mater*. 2009;8:621-629.
50. Watanabe M, Thomas ML, Zhang S, Ueno K, Yasuda T, Dokko K. Application of ionic liquids to energy storage and conversion materials and devices. *Chem Rev*. 2017;117:7190-7239.
51. Yan C, Yao YX, Chen X, et al. Lithium nitrate solvation chemistry in carbonate electrolyte sustains high-voltage lithium metal batteries. *Angew Chem Int Ed*. 2018;57:14055-14059.
52. Liu Y, Lin D, Li Y, et al. Solubility-mediated sustained release enabling nitrate additive in carbonate electrolytes for stable lithium metal anode. *Nat Commun*. 2018;9:3656.
53. Fan XL, Chen L, Ji X, et al. Highly fluorinated interphases enable high-voltage Li-metal batteries. *Chem*. 2018;4:174-185.
54. Fan X, Ji X, Han F, et al. Fluorinated solid electrolyte interphase enables highly reversible solid-state Li metal battery. *Sci Adv*. 2018;4:eaau9245.
55. Zhang XQ, Cheng XB, Chen X, Yan C, Zhang Q. Fluoroethylene carbonate additives to render uniform Li deposits in lithium metal batteries. *Adv Funct Mater*. 2017;27:1605989.
56. Zhao J, Liao L, Shi F, et al. Surface fluorination of reactive battery anode materials for enhanced stability. *J Am Chem Soc*. 2017;139:11550-11558.
57. Kim H, Wu FX, Lee JT, et al. In situ formation of protective coatings on sulfur cathodes in lithium batteries with LiFSI-based organic electrolytes. *Adv Energy Mater*. 2015;5:1401792.

58. Basile A, Bhatt AI, O'Mullane AP. Stabilizing lithium metal using ionic liquids for long-lived batteries. *Nat Commun.* 2016;7:11794.
59. Zhang R, Chen XR, Chen X, et al. Lithiophilic sites in doped graphene guide uniform lithium nucleation for dendrite-free lithium metal anodes. *Angew Chem Int Ed.* 2017;56:7764-7768.
60. Alpen U, Rabenau A, Talat GH. Ionic conductivity in Li₃N single crystals. *Appl Phys Lett.* 1977;30:621-623.
61. Rosenman A, Elazari R, Salitra G, Markevich E, Aurbach D, Garsuch A. The effect of interactions and reduction products of LiNO₃, the anti-shuttle agent, in Li-S battery systems. *J Electrochem Soc.* 2015;162:A470-A473.

SUPPORTING INFORMATION

Additional supporting information may be found online in the Supporting Information section at the end of this article.

How to cite this article: Yao Y-X, Zhang X-Q, Li B-Q, et al. A compact inorganic layer for robust anode protection in lithium-sulfur batteries. *InfoMat.* 2019;1–10. <https://doi.org/10.1002/inf2.12046>